Fiber-based joint time and frequency dissemination via star-shaped commercial telecommunication network*

Yi-Bo Yuan(袁一博)[1,2], Bo Wang(王波)[1,†], and Li-Jun Wang(王力军)[1,2]

[1] State Key Laboratory of Precision Measurement Technology and Instruments, Department of Precision Instrument, Tsinghua University, Beijing 100084, China

[2] Department of Physics, Tsinghua University, Beijing 100084, China

(Received 2 March 2017; revised manuscript received 30 March 2017; published online 20 June 2017)

A fiber-based, star-shaped joint time and frequency dissemination scheme is demonstrated. By working in cooperation with the existing commercial telecommunication network. Our scheme enables the frequency, time, and digital data networks to be integrated together and could represent an ideal option of interconnection among scientific institutions. The compensation functions of the time and frequency transfer scheme are set at the client nodes. The complexity of the central node is thus reduced, and future expansion by the addition of further branches will be accomplished more easily. During a performance test in which the ambient temperature fluctuation is 30 °C/day, timing signal dissemination stability is achieved to be approximately ±50 ps along 25-km-long fiber spools. After calibration, a timing signal synchronization accuracy of 100 ps is also realized. The proposed scheme offers an option of the construction of large-scale fiber-based frequency and time transfer networks.

Keywords: time synchronization, telecommunication network, frequency transfer, star-shaped network

PACS: 06.30.–k, 07.60.Vg, 06.30.Ft **DOI:** 10.1088/1674-1056/26/8/080601

1. Introduction

Precise time and frequency dissemination are of major importance for many scientific applications in areas such as comparison of frequency standards,[1] radio astronomy,[2] and deep space detection.[3] Because of turbulence and temperature fluctuations during free space dissemination, the stabilities of conventional frequency dissemination methods via satellite links are limited to the 10^{-15}/day level.[4] These types of methods can no longer satisfy the requirements for clock comparison applications below the order of 10^{-16}/day[5] or recent high-performance radio telescope arrays such as the Square Kilometer Array (SKA).[2] With its advantages of low attenuation, high reliability, and continuous availability, the existing fiber optic network has become an attractive option for use in such ultrahigh precision applications. In recent years, rapid progress has been made in fiber-based timing and frequency signal dissemination schemes. Schemes with a variety of different topological structures that are intended to meet various application requirements, ranging from point-to-point[6–14] to multi-access,[15–19] cascade,[20,21] and star-shaped[22,23] structures, have been demonstrated experimentally.

Recently, we developed a point-to-point simultaneous frequency transfer and time synchronization scheme,[9] and multi-access[15] and star-shaped frequency transfer schemes.[23] A multiple access timing signal synchronization scheme has also been demonstrated.[24] In addition to the realization of precise timing synchronization, the system error and its thermal drift were also calibrated. Using these results as a basis, we demonstrate a star-shaped timing signal synchronization scheme in this paper. By working cooperatively with our previously developed frequency transfer system,[25] a novel joint time and frequency dissemination system that is capable of working on commercial telecommunication networks is established. Unlike current star-shaped timing signal transfer schemes, which work in a wavelength-division multiplexing (WDM) mode, our timing synchronization scheme works on the basis of a time-division multiplexing pattern. The central node measures the round trip delay values for each of its branches and disseminates the delay value message to the client nodes via Ethernet connections by turns. In this way, the system error that is induced by the chromatic dispersion of the fiber links can be eliminated. More importantly, in the co-working mode of this scheme, the ultrahigh-precision frequency signals that are received at the client nodes can enhance the performance and the expandability of the timing synchronization system. The scheme can be regarded as a promising option of scientific research applications because it offers an effective integration of time, frequency and scientific data transfer networks.

In this paper, as a performance test for the proposed scheme, a simulative star-shaped joint time and frequency network is established using four 25-km-long fiber spools. In a

*Project supported by the National Key Scientific Instrument and Equipment Development Project, China (Grant No. 2013YQ09094303) and the Program of International Science and Technology Cooperation, China (Grant No. 2016YFE0100200).

†Corresponding author. E-mail: bo.wang@tsinghua.edu.cn

© 2017 Chinese Physical Society and IOP Publishing Ltd

test in which the ambient temperature of the fiber spools fluctuates by 30 °C/day, a timing signal dissemination stability of ±50 ps is achieved. After calibration of the systematic error that is caused by a combination of loop asymmetry and thermal drift, time synchronization accuracy of 100 ps is also realized. Additionally, the potential of this system for future large-scale extension and its adaptability to bad environments are also discussed.

2. Experimental scheme and setup

A schematic diagram of the complete fiber-based joint time and frequency dissemination system is shown in Fig. 1, and consists of one center node and two client nodes. In the central node, the time transmitting module and the frequency transmitting module are denoted by T-TX and F-TX, respectively, while in the two client nodes, the time and frequency receiving modules are denoted by T-RX and F-RX. To simulate a real telecommunication network scenario, three Ethernet switches are installed at three nodes. A S5500 Ethernet switch from H3C is placed at the central node, while the two client nodes are equipped with S2512 Ethernet switches from BDCOM. All three Ethernet switches are plugged into a 1310-nm double optical fiber SFP (small form-factor pluggable) transceiver module, and transmission and reception are realized using a single fiber pair. The transmissions of the timing and frequency signals use 1548.53-nm and 1547.72-nm laser beams as carriers, respectively. Therefore, with the eight WDMs and the four 25-km-long fiber spools connecting the three nodes, a star-shaped time and frequency network is established. The timing signal, the frequency signal and the Ethernet digital data can then be transmitted along the three different transmission channels without interactions among them.

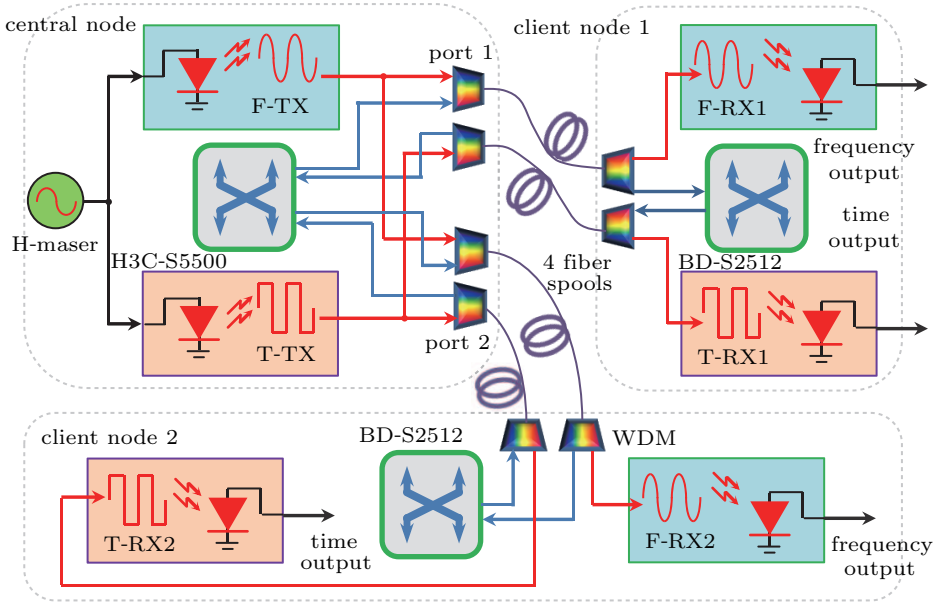


Fig. 1. (color online) Schematic illustration of the proposed joint time and frequency dissemination system using a commercial telecommunications network. H3C-S5500 and BD-S2512 are commercial Ethernet switches. T-TX: time transmitter module, T-RX: time receiver module. F-TX: frequency transmitter module, F-RX: frequency receiver module.

The frequency dissemination modules, F-TX and F-RX, almost work in the same way as the $1f$–$2f$ frequency dissemination scheme that was proposed originally in Ref. [23], but with greater robustness after the improvement which is described in detail in Ref. [25]. Our original star-shaped frequency dissemination scheme is susceptible to temperature fluctuations in the fiber links because of its limited isolation properties and the nonlinear effects of the radio-frequency components used. To make the proposed system suitable for scientific applications in severe environments, we design a nonharmonic synchronization scheme that is immune to dramatic temperature fluctuations. Additionally, to enhance the feasibility of the improved frequency transfer system, the dissemination modules F-TX and F-RX are integrated from discrete optical and microwave devices to form a homemade prototype. In this way, a joint time and frequency dissemination network can be established and can also be maintained more easily.

Figure 2 shows an outline of the scheme for the proposed star-shaped timing signal synchronization system. Taking the transfer link between T-TX and T-RX1 for example, a synthesized clock generator (SCG) that is referenced to an H-maser generates a 500-Hz timing signal with a 1:1 duty ratio at the T-TX. This generated timing signal is used to modulate the amplitude of the 1547.72-nm laser carrier wave via laser 1. The laser light is divided into two parts and these beams are sent to the two branches respectively. At T-RX1, the received timing signal is detected and is then sent to the delay fluctuation compensation system, which includes a controlled delay box (DG535, Stanford Research Systems) and a computer.

When triggered by the input pulse, the controlled delay box can recover and delay square pulses with 5-ps time delay resolution. The delayed timing signal is sent to laser 2 and is used to modulate the 1547.72-nm laser carrier beam. In this form, the signal is then sent back to T-TX. The optical switch (OSW12-1310E, Thorlabs) is used to transfer the loopback timing signals from the two branches to the detector by turns. The delay fluctuation detection system consists of a time interval counter (TIC; Keysight 53230A) and a computer. Using an optical switch, the round trip time delays of two branches are measured using the single TIC. The measured delay values are then disseminated to the corresponding time receiving modules via the Ethernet connections among the three nodes. The delay fluctuation compensation systems that are contained in the two time receiving modules can compensate for the fiber transfer delay fluctuations accordingly.

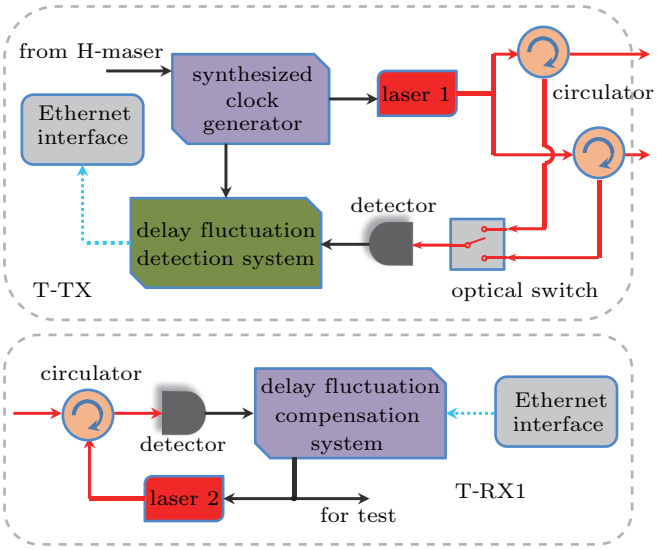


Fig. 2. (color online) Schematic illustration of star-shaped timing signal synchronization system.

Assuming that the uplink and downlink transmission time delays have equivalent values, the round trip delay is twice as long as the single trip delay. An iterative control algorithm is used to stabilize the recovered timing signal. If the single trip delay during the i-th control cycle is denoted by t_i, and the set delay value of the controlled delay box during the $(i-1)$-th control cycle is Δt_{i-1}, then the measured value at the TIC can be expressed as $T_i = \Delta t_{i-1} + 2t_i$. The set delay Δt_i of the controlled delay box is adjusted using an iterative relationship formula, which can be expressed as shown below

$$\Delta t_i = C + (\Delta t_{i-1} - T_i)/2. \tag{1}$$

From this, we can obtain $\Delta t_i + t_i = C$, where C is a constant value, and this is the time delay between the recovered timing signal and the clock signal at the center node. The T-RX1 and T-RX2 have their own control cycles and cycle ordinal numbers. T-TX transmits the TIC measurement results from each branch to the corresponding client nodes in turn. In the actual experiment, the starting value of Δt_0 is set at 10^5 ps, and the single trip delay C for both client nodes is set at 1.248×10^8 ps.

The control cycle period is highly significant as an experimental parameter. The control cycle period should cover the data acquisition time, the Ethernet transmission time and the instrument response time, and any other relevant time factors. To obtain better system performance, all these factors must be carefully balanced. For example, increasing the averaging time of the TIC would produce improved measurement resolution, but the system response time would also increase; meanwhile, a shorter response time may contribute little to the improvement of the system performance when the intrinsic jitter of electronic instruments such as the controlled delay box is taken into account. To ensure a sufficient margin in the experiments, the control cycle period for each client node is set at 2 s, and the T-TX disseminates the delay messages to each node by turns. By configuring the three Ethernet switches, the time synchronization control message is set to have the highest priority. In this way, the effects of Ethernet congestion can be greatly minimized for practical applications. Under some severe conditions, if there were no available Ethernet equipment, another alternative to communication channel such as telephone link or wireless telecommunication connection is necessary.

3. Results and discussion

In a joint timing signal and frequency dissemination system that is based on a commercial telecommunication network, the timing and frequency signals are highly vulnerable to the transmission link noise, while the digital Ethernet signal has a much greater anti-noise capability. When compared with buried fiber links, overhead fiber links offer several advantages, including shorter deployment times and lower infrastructure construction costs, but the transmission quality would be reduced. In certain scientific applications, overhead fiber links are used rather than buried links. Consequently, a joint robust timing and frequency dissemination system with high immunity to dramatic temperature fluctuations is required. The dissemination performances of the improved nonharmonic F-TX and F-RX modules are tested in the simulative telecommunication network. When the temperature fluctuates by 40 °C in one day, relative stabilities of approximately 4×10^{-14}/s and $3\times10^{-16}/10^4$ s are obtained.[25]

To test the timing signal dissemination system, the timing signals that are recovered at T-RX1 and T-RX2 are compared with the center node clock signal using a TIC (Keysight 53230A) with a 1-s averaging time. During the tests, two 25-km-long fiber spools are placed in a temperature-controlled box. The blackcurve shown in Fig. 3 indicates the free running round-trip delay fluctuation that occurs when the tem-

perature fluctuates between 15 °C and 40 °C. Over a single day, the round-trip delay fluctuation of a 25-km-long fiber link is approximately 40 ns. The test results for T-RX1 and T-RX2 are represented by the red and green curves shown in Fig. 3, respectively. The test results are normalized, which means that only the variation is expressed and the mean values are set to be zero. For the signal recovered from T-RX1, the peak-to-peak fluctuation is 124 ps, and the standard deviation is 10.4 ps, while for the signal recovered from T-RX2, the peak-to-peak fluctuation is 107 ps, and the standard deviation is 12.3 ps.

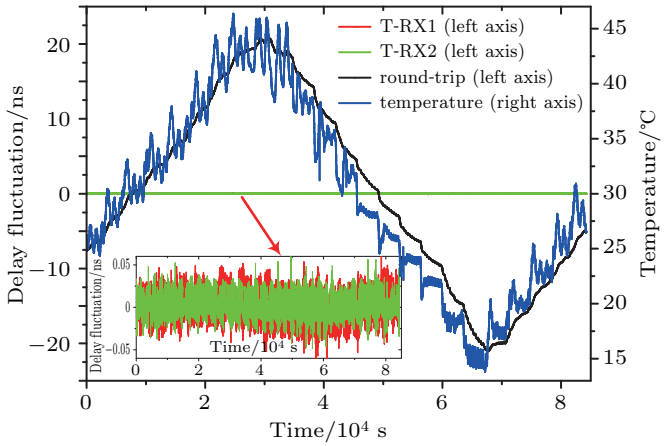


Fig. 3. (color online) Double *Y* plot of temperature and measured time delay fluctuations over a period of one day. Black curve: time delay fluctuation of free-running round trip transfer. Red curve: time delay fluctuation of the timing signal recovered from T-RX1. Green curve: time delay fluctuation of the timing signal recovered from T-RX2. Blue curve: temperature fluctuations of the fiber spools. Inset: fluctuation details of the timing signals recovered from T-RX1 and T-RX2.

Using the method described above, a highly stable timing signal can be obtained at each client node. However, to realize time synchronization, system errors such as the intrinsic dead time delay of the controlled delay box and the system transmission asymmetry caused by optical component delays in the T-TX or T-RX must be determined and eliminated because they could induce an inherent time difference between the recovered timing signal and the clock signal at T-TX. In Ref. [24], with the intention of promoting synchronization accuracy, the system errors and the thermal drift are calibrated and then compensated for. Finally, synchronization accuracy with a magnitude of 100 ps is achieved. In the current experiments, the two branches of the star-shaped timing signal synchronization system are calibrated in a similar manner. By short splicing of the T-TX and T-RX, the inherent time difference between the recovered timing signal and the clock signal is measured and recorded. The correction term that is derived from the recorded data can then be used to adjust the initial value Δt_0 of the controlled delay box. After correction, to test the timing signal accuracy, a series of timing signal dissemination experiments is performed using fiber spools of different lengths, varying from 0.1 km to 30 km, as performance tests. The time difference between the T-TX and the T-RX is measured using the TIC with a 1-s averaging time over a single day. The difference between the TIC measured value and the pre-set single trip delay C can be regarded as the system synchronization accuracy. The results of these tests are shown in Fig. 4, in which the mean value is used to draw each data point; the standard deviations of the acquired time data, which vary from 10.4 ps to 21.6 ps, are used to draw the error bars. After calibration, a time synchronization accuracy of 100 ps is realized using fiber links of various lengths.

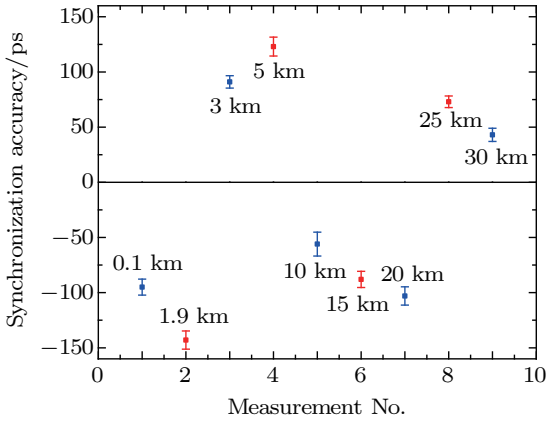


Fig. 4. (color online) Synchronization accuracy of star-shaped timing signal synchronization system. Red points: tests carried out using branch 1; blue points: tests carried out using branch 2.

Because the time synchronization system works in the time-division multiplexing mode, when the number of client nodes increases, the feedback speed may fail to catch up with the transfer delay fluctuations caused by the temperature fluctuations. When we consider that the optical switch that is used has only two available branches, different latency time lengths must be inserted into the control cycle of the T-RX to simulate multi-branch scenarios. For example, to simulate a network with N client nodes, an arbitrary client node must await an extra $2(N-1)$ s for the latest delay message from the center node. In such a case, the recovered timing signal would gradually drift away from the set value till the end of the latency time. The time difference between the recovered timing signal and the clock signal at the central node is measured using the TIC with a 1-s averaging time. The results are shown in Fig. 5 in the form of time deviation.

As shown in Fig. 5, with increasing latency time, the timing signal transfer system would not be able to compensate for the delay fluctuations caused by temperature fluctuations in real time, and thus the stability of the recovered timing signal would also deteriorate. Under these circumstances, a local timekeeping device located at each of the client nodes is of major importance. The frequency synchronization system can provide a frequency reference for the timekeeping device.

This timekeeping device then adjusts its phase based on the timing signal recovered from the T-RX when the node is in its own control cycle rather than in the latency time. When the set value Δt_i is updated, the time difference between the recovered timing signal and the local timekeeping SCG is measured immediately using a TIC. By adjusting the phase of the SCG accordingly in each control cycle, the time difference is then guaranteed to be smaller than the pre-set threshold value. For the clarity of expression, the output timing signal of the SCG at the client node after adjustment is called the 'reproduced timing signal'. In this way, after the adjustment and locking procedure, the reproduced timing signal would track the recovered timing signal closely. The stability of the reproduced timing signal would then be better than that of the recovered timing signal when the synchronized reference frequency signal is supplied to the SCG at the client node. The synchronization accuracy of the reproduced timing signal can be guaranteed to have the same order of magnitude as that of the recovered signal. In the performance test, the latency time is set at 158 s. Then, the time difference between the reproduced timing signal and the clock signal of the T-TX is measured and recorded when the reference signals of the SCG at the client node are different. The test results are shown in Fig. 6.

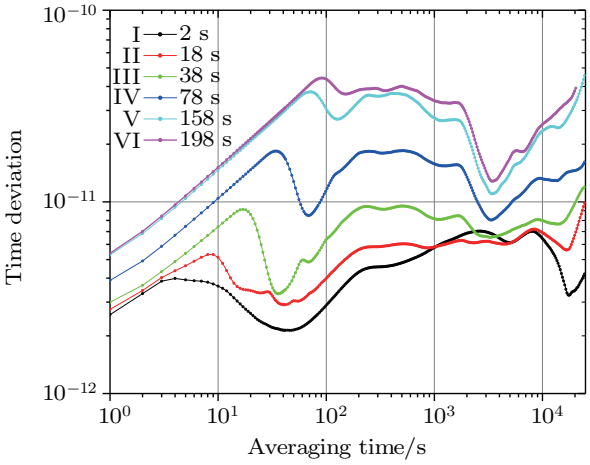


Fig. 5. (color online) Time deviations of the recovered timing signals for different latency times. Black curve I: latency time of 2 s. Red curve II: latency time of 18 s. Green line curve III: latency time of 38 s. Blue curve IV: latency time of 78 s. Cyan line V: latency time of 158 s. Magenta curve VI: latency time of 198 s. To show these lines more clearly, all tau modes in the Stable 32 software are selected when processing these data.

The stability of the reproduced timing signal is shown in Fig. 6 in the form of a time deviation. The red curve shows the reproduced timing signal stability when the SCG at the T-RX is referenced to the common reference of the T-TX. The green curve shows the reproduced timing signal stability when the SCG at the T-RX is referenced to the F-RX. Because of the excellent quality of the star-shaped frequency dissemination system, the compensated dissemination frequency-referenced timing signal shows no obvious difference when compared with the corresponding common clock-referenced signal; additionally, the performance of the reproduced timing signal is approximately one order of magnitude better than that of the recovered signal in a simulative star-shaped network with 80 branches. The efficient integration of the time and frequency dissemination network makes it possible to maintain good timing signal performance as the number of branches increases. In this way, the network expandability towards larger scale systems is enhanced.

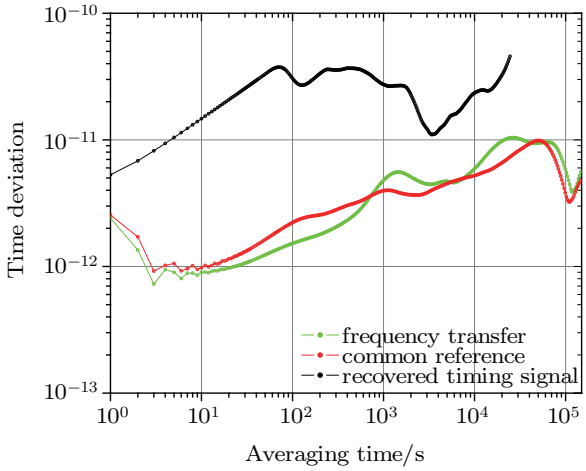


Fig. 6. (color online) Time deviations of reproduced timing signals versus averaging time. Red curve: the SCG at the T-RX is referenced to the common reference of the T-TX. Green curve: the SCG at the T-RX is referenced to the frequency signal that is recovered from the F-RX. Black curve: the performance of the recovered timing signal recovered when the latency time is 158 s (for comparison). All tau modes in the Stable 32 software are also selected when processing these data.

4. Conclusions and perspectives

In this work, we introduce a high-precision optical fiber-based joint time and frequency dissemination method. Under severe conditions involving dramatic temperature fluctuations, frequency transfer stability of 4×10^{-14}/s and timing signal dissemination stability of ± 50 ps are achieved along 25-km-long fiber spools. After calibration, synchronization accuracy of 100 ps is also realized. Our scheme demonstrates excellent applicability and practicality to provide excellent compatibility with commercial telecommunication networks. The proposed scheme could provide an easy way to interconnect scientific application users via the dark fibers of the network infrastructure. Because of merits such as high precision, low cost, high robustness and its great capacity for future extension, this scheme could provide a new insight into the construction of fiber-based time and frequency transfer networks.

References

[1] L Foreman S M, Holman K W, Hudson D D, Jones D J and Ye J 2007 *Rev. Sci. Instrum.* **78** 021101

[2] Turner W SKA phase 1 system (level 1) requirement specification. Available at: https://www.skatelescope.org/keydocuments/

[3] Lau K Y, Lutes G F and Tjoelker R L 2014 *J. Lightw. Technol.* **20** 3440
[4] Levine J 2008 *Metrologia* **49** 772
[5] Jiang Y Y, Ludlow A D, Lemke N D, Fox R W, Sherman J A, Ma L S and Oates C W 2011 *Nat. Photon.* **5** 158
[6] Predehl K, Grosche G, Raupach S M F, Droste S, Terra O, Alnis J, Legero T, Hänsch T W, Udem T, Holzwarth R and Schnatz H 2012 *Science* **336** 441
[7] Williams P A, Swann W C and Newbury N R 2008 *J. Opt. Soc. Am. B* **25** 1284
[8] Fujieda M, Kumagai M, Nagano S, Yamaguchi A, Hachisu H and Ido T 2011 *Opt. Express* **19** 16498
[9] Wang B, Gao C, Chen W L, Miao J, Zhu X, Bai Y, Zhang J W, Feng Y Y, Li T C and Wang L J 2012 *Sci. Rep.* **2** 556
[10] Rost M, Piester D, Yang W, Feldmann T, Wübbena T and Bauch A 2012 *Metrologia* **49** 772
[11] Wu G L, Hu L, Zhang H and Chen J P 2014 *Rev. Sci. Instrum.* **85** 114701
[12] Śiwczynski Ł, Krehlik P and Lipiński M 2010 *Meas. Sci. Technol.* **21** 075302
[13] Ning B, Zhang S Y, Hou D, Wu J T, Li Z B and Zhao J Y 2014 *Sci. Rep.* **4** 5109
[14] Chen X, Zhang J, Lu J L, Lu X, Tian X S, Liu B, Wu H, Tang T S, Shi K B and Zhang Z G 2015 *Opt. Lett.* **40** 371
[15] Gao C, Wang B, Chen W L, Bai Y, Miao J, Zhu X, Li T C and Wang L J 2012 *Opt. Lett.* **37** 4690
[16] Grosche G 2014 *Opt. Lett.* **39** 2545
[17] Zhu X, Wang B, Gao C and Wang L J 2016 *Chin. Phys. B* **25** 090601
[18] Jiang Z, Dai Y T, Zhang A X, Yin F F, Li J Q, Xu K, Lv Q, Ren T P and Tang G S 2015 *IEEE Photon. J.* **7** 2
[19] Śiwczynski Ł and Krehlik P 2015 *IEEE Trans. Ultrason. Ferroelectr. Freq. Control* **62** 412
[20] Fujieda M, Kumagai M and Nagano S 2010 *IEEE Trans. Ultrason. Ferroelectr. Freq. Control* **57** 168
[21] Gao C, Wang B, Zhu X, Yuan Y B and Wang L J 2015 *Rev. Sci. Instrum.* **86** 093111
[22] Schediwy S W, Gozzard D, Baldwin K G H, Orr B J, Warrington R B, Aben G and Luiten A N 2013 *Opt. Lett.* **38** 2893
[23] Wang B, Zhu X, Gao C, Bai Y, Dong J W and Wang L J 2015 *Sci. Rep.* **5** 13851
[24] Yuan Y B, Wang B, Gao C and Wang L J 2017 *Chin. Phys. B* **26** 040601
[25] Zhu X, Wang B, Guo Y C, Yuan Y B, Gamatham R, Wallace B, Grainge K and Wang L J 2017 arXiv: 1702.06599 [ph.ins-det]